Materials Science and Engineering B 282 (2022) 115789

Contents lists available at ScienceDirect

Materials Science & Engineering B

journal homepage: www.elsevier.com/locate/mseb

Biosynthesized zinc oxide nanoparticles using seed and bark extract of *Azadirachta indica* for antibacterial, photocatalytic and supercapacitor applications

Mona Saini [a], Sapna Yadav [a], Nutan Rani [a], Asifa Mushtaq [b], Seema Rawat [c], Kalawati Saini [a,*], Dipak Maity [d,*]

[a] Department of Chemistry, Miranda House, University of Delhi, Patel Chest Marg, New Delhi 110007, India
[b] Department of Botany and Microbiology, H.N.B. Garhwal University, Srinagar 241674, Uttarakhand, India
[c] School of Life Sciences, Central University of Gujarat, Sector- 30, Gandhinagar 382030, Gujarat, India
[d] Department of Chemical Engineering, University of Petroleum and Energy Studies, Dehradun 248001, India

ARTICLE INFO

Keywords:
Bio-synthesis
Zinc oxide nanoparticles
Azadirachta indica
Antibacterial
Photocatalytic activity and Supercapacitor

ABSTRACT

We have reported biosynthesis of zinc oxide (ZnO) nanoparticles (NPs: S3/B3) using an aqueous extract of seeds and barks of *Azadirachta indica* for antibacterial, photocatalytic, and supercapacitor applications. XRD pattern demonstrates a hexagonal wurtzite structure while FTIR spectra confirm the phytochemicals coating. Morphology is revealed from the FE-SEM images: (a) block-shaped S3 with ~ 50–100 nm width and 90–125 nm length; (b) bar-shaped B3 with ~ 40–50 nm thickness and 200 nm length. DLS study showed a zeta potential value of −28.93/-28.00 mV for S3/B3 indicating their good colloidal stability in aqueous suspension. Besides, antimicrobial activity of S3 is performed on various gram-negative/-positive bacteria and minimum inhibitory concentrations (MIC) are determined as 125–150 μg/mL. Moreover, methyl orange dye has been degraded with B3 NPs with a degradation efficiency of 84.62% in 180 min. Furthermore, the specific capacitance (C_s) and energy density (E) values of the S3/B3 confirmed their potentiality for supercapacitor applications.

1. Introduction

Nowadays, transition metal oxides nanoparticles (MONPs) have attracted a great deal of attention because of their excellent chemical stability and numerous physicochemical properties [1–5]. Among these, zinc oxide (ZnO) nanoparticles (NPs) and their nanocomposites are extensively used in potential multifunctional applications such as photocatalytic [6], supercapacitor [7], wound healing [8], gas sensing [9], anti-bacterial/fungal [10], opto-/piezo-electronic [11–12], anticancer and other biomedical applications [13–14]. Nanostructures of ZnO are also studied for theranostics and drug delivery [15].

Recently, ZnO NPs have received considerable attention as antibacterial agents due to their toxic effect on various bacteria such as *Escherichia coli* [16–17]. Sharmila et al *have* reported biosynthesized ZnO NPs using leaves extract of *Tecoma castanifolia* for antimicrobial and anticancer activity [18]. Similarly, Ramesh *et al* have synthesized ZnO NPs using leaves extract of *Solanum nigrum* for antimicrobial activity [19]. Later, Zhong et al reported the ultrahigh efficiency of ZnO nanorods for antibacterial activity [20]. Moreover, ZnO NPs are biosynthesized using flower extract of *Trifolium pratense* for antibacterial study [21]. Likewise, ZnO NPs are also biosynthesized using seed extract of *Silybum marianum* for antibacterial and antidiabetic activity [22]. Recently, Asif et al. have biosynthesized ZnO NPs using cyanobacteria for a bioactivity study and compared them with commercially available ZnO [23].

Nowadays, ZnO and Zinc ferrite NPs and their nanocomposites are widely investigated as photocatalysts for photocatalytic degradation of various organic dyes under the irradiation of light [24–25]. For example, Lv et al have investigated the photocatalytic activity of ternary composite of ZnO NPs with reduced graphene oxide (rGO) and carbon nanotube (CNT) for degradation of methylene blue [25]. Similarly, Gao et al have studied the rapid photodegradation of Rhodamine B (RhB) in presence of visible light with a nanocomposite of ZnO NPs functionalized with sulphonated graphene oxide (SGO) [26]. Likewise, Gu et al have synthesized the coral-like composites of ZnO/C-$ZnFe_2O_4$ hierarchical structures to enhance photocatalytic as well as antibacterial

* Corresponding authors.
E-mail addresses: kalawati.saini@mirandahouse.ac.in (K. Saini), dipakmaity@gmail.com (D. Maity).

https://doi.org/10.1016/j.mseb.2022.115789
Received 16 April 2022; Received in revised form 7 May 2022; Accepted 17 May 2022

efficiency [27].

Currently, MONPs are extensively used for high-performance supercapacitor applications due to their low resistance [28–34]. Yadav et al have reported a comparative study of biosynthesized ZnO NPs and CuO NPs for electrochemical supercapacitor applications [35]. Similarly, Singh et al have studied nanocomposite of ZnO NPs for supercapacitor application and reported the specific capacitance (C_s) value of 100 mF/cm^2 which is stable up to 2000 cycles [36]. Rani et al have reported a specific capacitance (C_s) value of 535.7142F/g at a voltage scan rate of 20 mV/s for biosynthesized rod-shaped ZnO nanostructure using glassy carbon electrode [7]. Likewise, Justin et al obtained a C_s value of 5 mF/cm^2 for core/shell ZnO/MnO_2 nanocomposite in 1 M Na_2SO_4 aqueous supporting electrolyte [28]. Saghafi et al have reported the specific capacitance (C_s) value of 1237F/g at 50 mV/s using bimetallic oxide Zn-Co electrode [29].

In this work, we have biosynthesized ZnO NPs using an aqueous extract of seeds and barks of *Azadirachta indica* (neem tree) for antibacterial, photocatalytic, and supercapacitor applications. Herein, the seeds/barks extract consists of various phytochemicals that act as a reducing agent as well as a capping/stabilizing agent. As-synthesized ZnO NPs are investigated for antimicrobial activity against four bacteria such as *Pseudomonas aeruginosa*, *Escherichia coli*, *Staphylococcus aureus* and *Streptococcus pneumonia*. ZnO NPs are also inspected for photocatalytic degradation of methyl orange (MO) dye under UV light. Moreover, the electrochemical study of biosynthesized ZnO NPs has been performed via cyclic voltammetry (CV) using 0.5 M Na_2SO_4 electrolytes.

2. Materials and methods

The metal salt precursor, zinc sulfate heptahydrate ($ZnSO_4{\cdot}7H_2O$), and sodium hydroxide (NaOH) are obtained from Central Drug House (P) Ltd – CDH, India. Methyl orange dye is procured from Merck, and supporting electrolyte sodium sulfate (Na_2SO_4) is acquired from Sigma Aldrich. All solutions are prepared in double-distilled water. All the reaction precursors and the supporting electrolyte are of analytical grade (A.R.).

2.1. Collection of neem tree seeds and barks

Healthy and fresh seeds and barks of *Azadirachta indica* (Neem tree) are collected from the Department of Chemistry, University of Delhi.

2.2. Preparation of 25% of seeds and barks extract

The seeds and barks of *Azadirachta indica* are washed with double distilled water and dried in a hot air oven for 2 h at 60 °C. The amount of 25 g of seeds/barks in powdered form is added to 100 mL of double-distilled water and then kept on a hot plate magnetic stirrer for half an hour at 40 °C. Next, the freshly prepared extract is filtered using the Whatman filter paper no.1, after that filtered extracts are added to the corresponding reaction precursor's solutions for the synthesis of ZnO NPs.

2.3. Synthesis of ZnO NPs

ZnO NPs are synthesized via a green approach using seeds and barks extract of *Azadirachta indica* and the as-prepared ZnO NPs samples are labeled as S3 and B3, respectively. Herein, 50 mL aqueous solution (0.2 M) of pure $ZnSO_4{\cdot}7H_2O$ and 50 mL aqueous solution (1.0 M) of NaOH are taken in a beaker and then 3 mL freshly-prepared seeds/barks extract is added into this beaker containing zinc precursor solution. Next, the resulting reaction mixture is heated and maintained at 40 °C (313 K) while constantly stirred at 450 rpm for two hours using a hot plate magnetic stirrer. As a result, ZnO NPs are precipitated from the reaction mixture with a formation of white-colored colloidal solution. Subsequently, the precipitated ZnO NPs are centrifuged and washed with 90% alcohol. After that, the washed ZnO NPs are dried at 80 °C in a hot air oven for two hours and the dried powder samples (S3/B3) are further characterized.

2.4. Characterization of ZnO NPs

The UV–Visible absorption spectra of the as-synthesized ZnO NPs (S3/B3) are recorded by UV-Spectramax M2e UV–visible spectrophotometer. The composition of the S3/B3 is determined via Fourier transform infrared (FT-IR) spectroscopy (using 55-Spectrometer, Bruker, USA) with the KBr pellet as the reference material. The crystal structure of the ZnO NPs is determined from the X-ray diffraction (XRD) pattern obtained by an X-ray diffractometer (D8 Discover, Bruker) equipped with Cu K_α (as X-ray source, $\lambda = 1.54056$ Å), where 2θ value is kept in the range of $25^\circ - 80^\circ$ (with an increment of 0.0194°/s). Surface topography/morphology of the as-prepared ZnO NPs are determined by using a scanning electron microscope (JEOL Japan Mode: JSM 6610LV) with 30 kV accelerating voltage and magnifications: X5 to X 3,00,000 at a resolution of 3 nm under high vacuum, whereas elemental composition is determined through in-built energy-dispersive X-ray spectroscopy (EDS). Further, the zeta potential values of an aqueous suspension of the S3/B3 samples are recorded using the dynamic light scattering (DLS, Horiba Nano ZS) technique.

2.5. Antibacterial activity

The antibacterial activity of as-synthesized ZnO NPs (S3) is performed via broth dilution method (Garcia, 2010) [37] using the stains from clinical isolates and the bacteria such as *Escherichia coli, Pseudomonas aeruginosa, Staphylococcus aureus* and *Streptococcus pneumoniae.* Initially, a stock solution of NPs (2 mg/mL) is prepared by dispersing ZnO NPs (S3) in pre-sterilized deionized water using ultra-bath sonicator. Next, the stock solution is further diluted to different concentrations ranging from 0.2 μg/mL to 200 μg/mL and then added into the test tubes containing varying amounts of sterile Luria Bertani broth (Muniyan et al., 2017) [38].

After that, 0.5 mL of overnight culture test bacteria (using 0.5 McFarland turbidity standards) are added to these test tubes aseptically and later the tubes are incubated at 37 °C for 24 h. The bacterial cultures without any test solution and the tubes with only sterile media are kept as positive and negative controls, respectively. Finally, the results are obtained by measuring the optical density of the inoculated broth at 600 nm while minimum inhibitory concentration (MIC) is recorded as the lowest concentration of the test sample inhibiting the growth of the inoculated test bacteria.

2.6. Photocatalytic activity

The photocatalytic experiment is performed using a Lelesil Innovative Photocatalytic Reactor. Herein, 500 mL methyl orange solution (2 μM in neutral medium pH = 7.0) is exposed to a 125 W low-pressure mercury lamp for 180 min in presence of 250 mg of ZnO NPs (B3) as a nanocatalyst for methyl orange degradation. Next, 4 mL of dye samples are taken out from the test solution initially at a 20 min interval up to 60 min and then at a 30 min interval. Each sample is centrifuged for 4 min at 1200 rpm and the maximum absorbance is recorded at 464.58 nm (λ_{max}) using a spectrophotometer (Model: SpectraMaxM2e). Herein, the absorbance for dye test solution is decreased with time continuously after exposure to UV–Visible light.

2.7. Electrochemical analysis

Electrochemical analysis of the as-prepared ZnO NPs is performed using an electrochemical work-station (Model: K-Lyte 1.2) at room temperature and applying a three-electrode system (Pt electrode as

working electrode (NPs are drop casted on it), Ag/AgCl as reference electrode, Pt mesh as a counter electrode). Herein, specific capacitance (C_s) is calculated using the cyclic voltammetry (CV) technique. This study has been done in presence of 0.5 M Na_2SO_4 at different scan rates at 20 mV/s, 40 mV/s, 60 mV/s, 80 mV/s and 100 mV/s respectively.

3. Results and discussions

3.1. UV–Visible spectroscopy

Fig. 1(a) shows the UV–Visible spectra of the as-synthesized ZnO NPs (S3/B3) and the maximum absorbance are obtained at 369.03 nm and 367.52 nm for S3 and B3 samples, respectively. Similar values of maximum absorption peak (λ_{max}) are reported by Khara et al, Padalia et al and Jayaseelan et al [39–41]. The energy bandgap (E_g) is evaluated from the intercepts of tauc's plots (i.e. $(\alpha h\nu)^2$ vs $h\nu$ curves using UV–Vis absorption spectra data) as shown in Fig. 1(b) and Fig. 1(c) for S3 and B3 samples, respectively. The tauc's formula (equation 1) is used to evaluate the energy bandgap as follows, where A denotes a constant and $h\nu$ represents the photon energy. The value of γ factor is equal to 1/2 for the direct and 2 for indirect transition energy bandgaps respectively.

$$(\alpha h\nu)^{1/\gamma} = A(h\nu - E_g) \quad (1)$$

Herein, the E_g value is determined as 2.8192 eV and 2.4772 eV for S3 and B3, respectively. Thus, the E_g value for S3 is found to be greater than that of the B3 indicating that the capping efficiency of phytochemicals present in seed extract is higher than that of phytochemicals present in the barks extract *of Azadirachta indica*. These results are in good agreement with the reported values by Rani et al [7] and other groups [6,42]. Besides, Robels et al have observed that the E_g value decreases from 2.96 eV to 2.77 eV with increasing concentration of *Hibiscus sabdariffa* extract for the synthesis of ZnO NPs [43].

3.2. FTIR analysis

Fig. 2 (a) and 2 (b) depict the FTIR spectra of the as-synthesized S3 and B3 samples in the wavenumber range of 4000–500 cm^{-1} and 1600–400 cm^{-1}, respectively.

Fig. 2 (a) shows the broad peak at 3326.60 cm^{-1} and 3500,16 cm^{-1} –3390.24 cm^{-1} for stretching/bending vibration of OH group due to physically adsorbed water (H_2O) molecules to the S3 and B3 NPs, respectively. Similar results have been reported in the literature [41,7]. Fig. 2 (b) portrays the peaks at 1550.48 cm^{-1} and 1508.43–1425.13 cm^{-1} due to the presence of carboxylic C = O group indicating phytochemicals (such as polyphenolic acid, derivative of polyphenolic acid, flavonoids and so on) attached to the ZnO NPs of the S3 and B3 NPs, respectively. Besides, the peaks corresponding to the aromatic -C-H bond (1095.41–1041.37 cm^{-1}), -C-O bond (1378.85 cm^{-1}), aromatic -C = C (1498.41–1475.27 cm^{-1}) are representing phytochemicals attached to the S3 sample. Likewise, the bands conforming to the aromatic -C-H bond (1095.36–1041.37 cm^{-1}, 944.94–887.09 cm^{-1}), -C-O bond (1374.99 cm^{-1}), aromatic -C = C (1426.13 cm^{-1}) are also demonstrating phytochemicals attached to the B3 NPs. Moreover, the peaks at 835.95–617.10 cm^{-1} and 827.31–632.53 cm^{-1} are due to the -Zn-O- stretching vibrations of the S3 and B3 NPs, respectively.

3.3. X-ray diffraction (XRD) analysis

Fig. 3 shows the XRD pattern of the as-synthesized S3/B3 NPs and matched with that for the ZnO NPs as reported by Seo et al, Salehi et al and Akhtar et al (JCPDS No. 5–0664, 36–1451) [5,44–45]. The peaks corresponding to the 2θ values of 31.28°, 34.04°, 36.04°, 47.09°, 56.17°, 62.32°, 66.01°, 67.48°, 68.63°, 72.18° and 76.48° are due to the (*hkl*) as (100), (002), (101), (102), (110), (103), (200), (112), (201), (004) and (202) confirms the wurtzite crystalline structure of S3/B3 NPs.

3.4. FE-SEM and EDS analysis

Fig. 4 (a) and 4 (b) show the FE-SEM images of the as-prepared B3 and S3 samples, respectively. It can be seen that the obtained ZnO NPs are bar shaped with ~ 40–50 nm thickness and 200 nm length and block shaped with ~ 50–100 width and 90–125 nm length for the B3 and S3 samples, respectively. Besides, the ZnO nanobars (B3) are stacked with a parallel alignment whereas ZnO nanoblocks (S3) are agglomerated as shown in Fig. 4(a) and 4 (b), respectively.

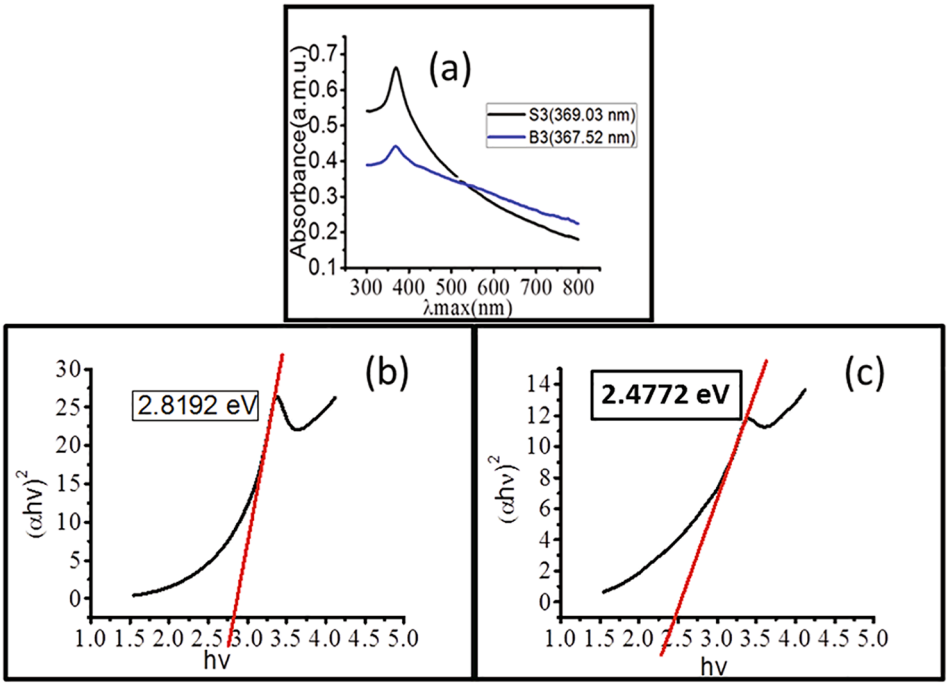

Fig. 1. (a) UV–Visible absorption spectra for S3 and B3 samples, (b) Tauc's plots of S3 sample (E_g = 2.8192 eV), (c) Tauc's plots of B3 sample (E_g = 2.4772 eV).

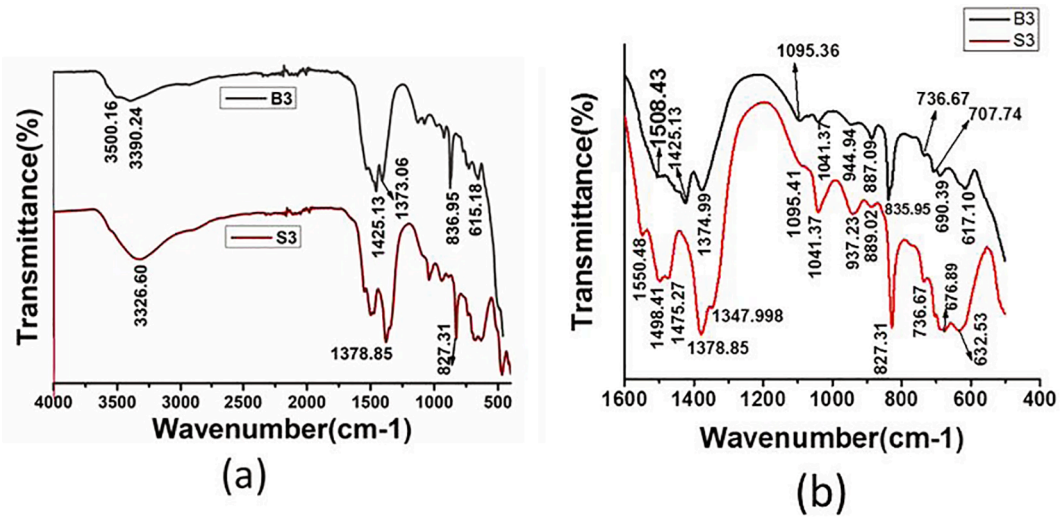

Fig. 2. FTIR Spectra of the as-prepared ZnO NPs (S3/B3) in the wavenumber range of (a) 4000 cm^{-1} –500 cm^{-1} and (b) 1600 cm^{-1} –400 cm^{-1}.

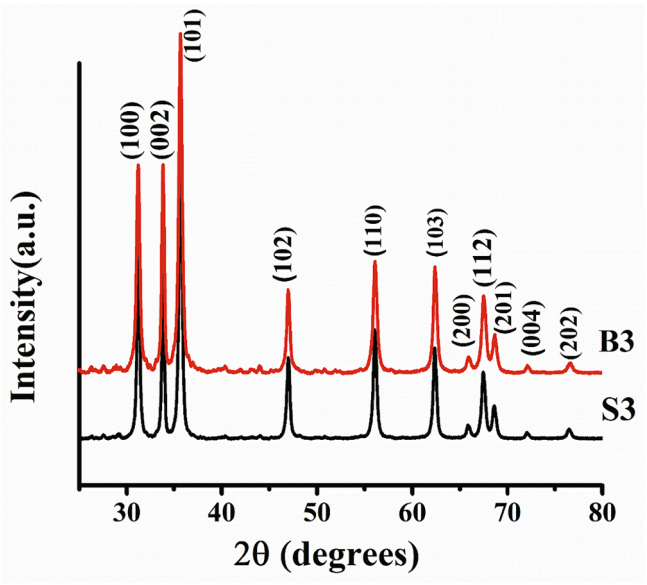

Fig. 3. X-ray diffraction pattern of the as-synthesized S3 and B3 samples.

3.5. Zeta potential analysis

Fig. 5 represent the zeta potential curves of the as-synthesized ZnO NPs dispersed in an aqueous suspension. The zeta potential value is determined as −28.93 mV for S3 and −28.00 mV for B3 as shown in Fig. 5 (a) and 5 (b), respectively, thus, indicating the good colloidal stability of the ZnO NPs in their aqueous dispersion. Similar zeta potential values are reported by Asif et al. (–22.1 mV), Akhtar et al. (-31 mV) and Asik et al (-28.2 mV) for the aqueous suspension of the green synthesized ZnO NPs [23,45,46]. Such type of stability based on zeta potential is applicable for biomedical application of these green synthesized ZnO NPs in future.

3.6. Antibacterial activity

Herein, the antimicrobial activity of as-synthesized ZnO NPs (S3) are performed using the broth dilution method on two different types of bacteria namely (i) gram-negative bacteria (*Escherichia coli* and *Pseudomonas aeruginosa*) and (ii) gram-positive bacteria (*Staphylococcus aureus* and *Streptococcus pneumoniae*) and the results are given in Table 1. The minimum inhibitory concentration (MIC) is found to be 135 μg/mL for *Escherichia coli*, 150 μg/mL for *Pseudomonas aeruginosa*, and 125 μg/mL for both *Staphylococcus aureus* and *Streptococcus pneumonia*, respectively. It is clear from the MIC values that as-synthesized ZnO NPs (S3) are more effective against gram-positive clinical isolates than gram-negative clinical isolates. Moreover, higher MIC values are demonstrated for gram-negative bacteria indicating that these clinical

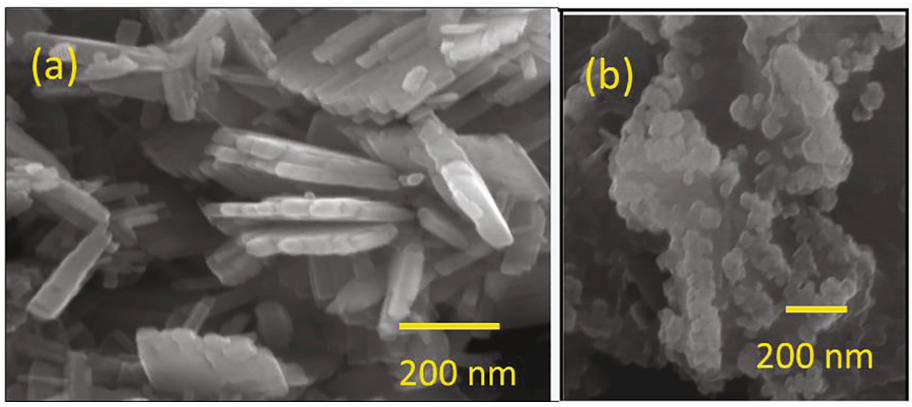

Fig. 4. FE-SEM images of as-synthesized ZnO NPs: (a) B3 (with bark extract) and (b) S3 (with seeds extract).

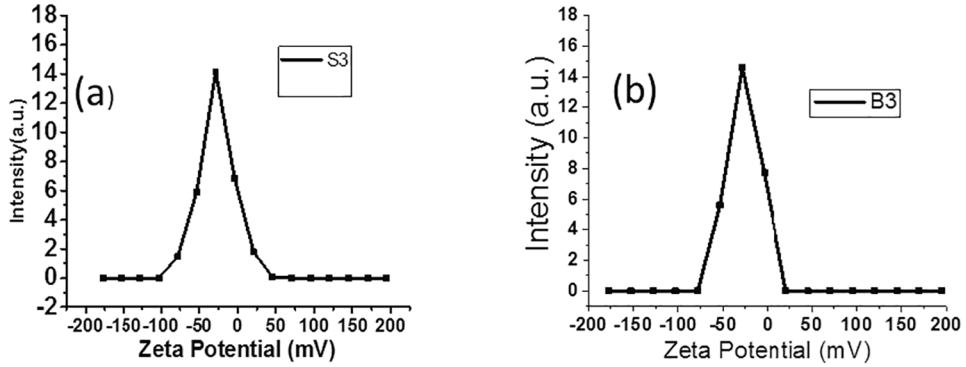

Fig. 5. Zeta potential curves of (a) ZnO NPs (S3) synthesized with seeds extract and (b) ZnO NPs (B3) synthesized with barks extract.

Table 1
Minimum Inhibitory Concentration (MIC in μg/mL) of as-prepared ZnO nanoparticles (S3) for various bacterial pathogens.

S.N.	Clinical Isolates	MIC value (μg/mL)
1	*Escherichia coli*	135
2	*Pseudomonas aeruginosa*	150
3	*Staphylococcus aureus*	125
4	*Streptococcus pneumoniae*	125

isolates are more resistant against the as-synthesized ZnO NPs (S3) i.e., a higher concentration of ZnO NPs is needed to prevent the growth of these microbes. Table 2 shows the reported MIC values for antibacterial activities of green synthesized ZnO NPs (using extract of various parts of different types of plants) against various gram-positive as well as gram-negative bacteria [47–53].

It is clear that as-synthesized ZnO NPs are more effective towards gram-negative bacteria whereas MIC value (125 μg/mL) has been found to be half of the reported value (i.e., 250 μg/mL by Barani et al) for *Staphylococcus aureus* [53]. The higher MIC values for gram-negative bacteria than gram-positive bacteria can be explained on the basis of strongly negative charge to surface of gram negative bacterial cells. As we know that the gram negative bacteria have an outer covering of bacterial cell wall structure. This cell wall structure is made of lipopolysaccharides and phospholipids respectively. The surface of gram negative bacterial cells have negative charge due to presence of lipopolysaccharides. The negative zeta potential (-28.93 mV) of synthesized nanoparticles (S3) can be responsible for higher value of MIC. Due to negative zeta potential the interaction between synthesized nanoparticles and surface of bacterial cells wall will be lesser than the gram positive bacterial cells. So, the lipopolysaccharides present in cell wall structure of gram-negative bacteria that make the cell wall more resistant and impermeable to external substances, such as antibacterial agents. World health organization (WHO) has also published a list of antibiotic-resistant priority for gram negative pathogens in 2017 [73].

Similarly, high value of MIC for gram negative bacteria than gram positive bacteria is reported by Al-nemrawi et al [74]. The authors reported that ZnO NPs have MIC value of 100 μg/mL against E. coli (gram negative bacteria) and 50 μg/mL against S. aureus (gram positive bacteria).

3.7. Photocatalytic activity

Fig. 6 (a) depicts UV–Visible spectra for photocatalytic degradation of methyl orange (MO) in presence of nanocatalyst ZnO NPs (B3) at different time intervals and without B3 (MO blank - black colour curve). Herein, the absorbance of MO at λ_{max} (464.58 nm) is assigned respectively as A_o in absence of nanocatalyst and A_t in presence of nanocatalyst for the MO sample taken out from the test solution at different times

Table 2
Comparison of antibacterial activities of earlier reported biosynthesized ZnO NPs.

S. N.	Nanoparticles	Plant extract/ Bacteria used	Organism/ MIC value	References
1	ZnO	*Brassica rapa*	*Escherichia coli*/25 μg/mL *Bacillus subtilis*/ 12.5 μg/mL	[47]
2	5% Ni-ZnO	*Brassica rapa*	*Escherichia coli*/25 μg/mL *Bacillus subtilis*/50 μg/mL	[47]
3	ZnO	*Berberis aristata*	*Escherichia coli*/256 μg/mL *Klebsiella pneumonia*/256 μg/mL	[48]
4	ZnO	*Periconium* sp.	*Staphylococcus aureus*/50 μg/mL *Escherichia coli*/50 μg/mL	[49]
5	ZnO	*Medicago sativa*	*Staphylococcus epidermidis* 0.58 μg/mL	[50]
6	ZnO	*Prosophis fracta*	*Pseudomonas aeruginosa*/12.5 μg/mL *Acinetobacter baumannii*/12.5 μg/mL	[51]
7	Ag-ZnO	*Prosophis fracta*	*Pseudomonas aeruginosa*/3.12 μg/mL *Acinetobacter baumannii*/3.12 μg/mL	[51]
8	ZnO	*Stachytarpheta jamaicensis*	*Staphylococcus aureus*/ < 25 μg/mL *Bacillus subtilis*/ < 25 μg/mL	[52]
9	5% Cu-doped ZnO	*Stachytarpheta jamaicensis*	*Staphylococcus aureus*/ < 25 μg/mL *Bacillus subtilis*/50 μg/mL *Escherichia coli*/125 μg/mL	[52]
10	ZnO	*Marinobacter* sp. *And Vibrio* sp.	*Pseudomonas aeruginosa*/62.5 μg/mL *Staphylococcus aureus*/250 μg/mL *Bacillus subtilis*/500 μg/mL *Listeria innocua*/ 1000 μg/mL	[53]

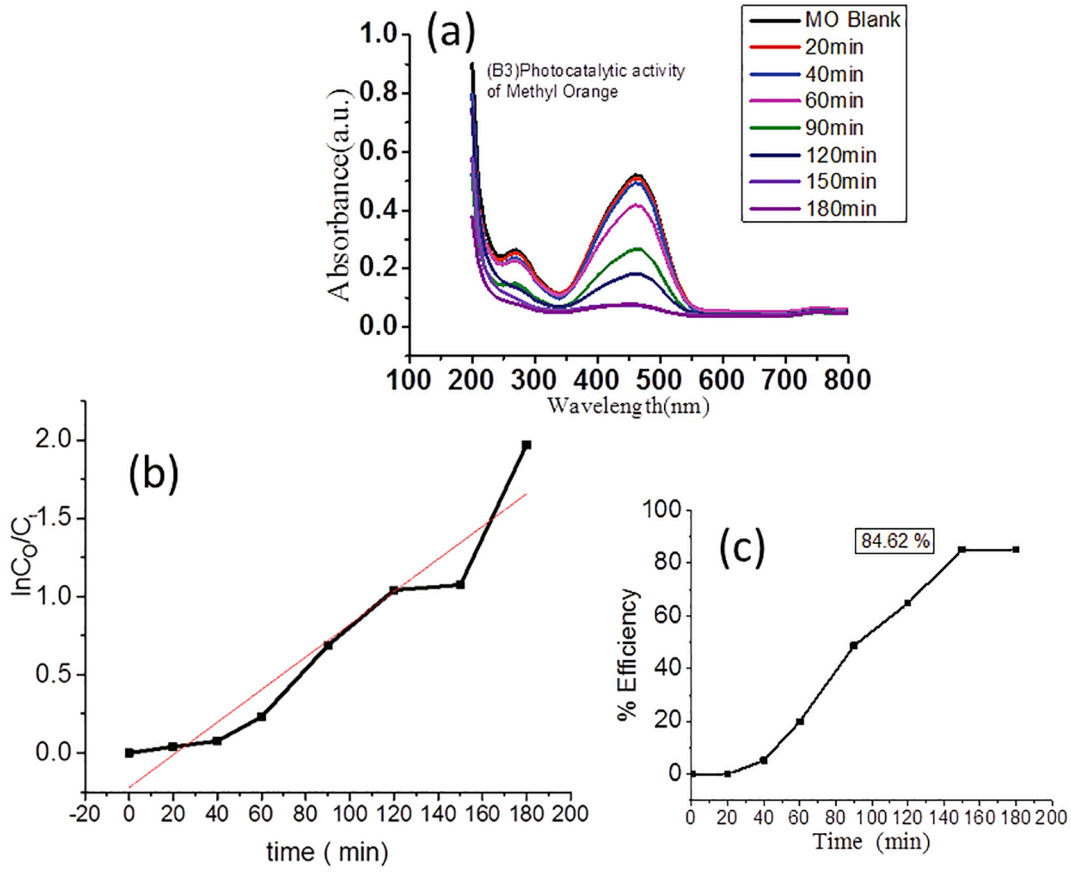

Fig. 6. (a) UV–Visible spectra for degradation of methyl orange in presence of nanocatalyst ZnO NPs (B3) at different time intervals and without catalyst (MO blank), (b) Methyl orange degradation kinetics: $\ln \frac{C_o}{C_t}$ vs time (min), (c) Methyl orange degradation efficiency (%) using ZnO NP (B3) vs time (min). (For interpretation of the references to colour in this figure legend, the reader is referred to the web version of this article.)

intervals up to 180 min after UV–Visible light exposure. It is clear from Fig. 6 (a) that no new λ_{max} peak arises at different time intervals of dye degradation. It indicates that the MO is completely degraded into water and carbon dioxide with time in presence of the light. According to Lambert-Beer's law absorbance is directly proportional to concentration and hence absorbance is respectively considered as A_o (absorbance of stock solution) and A_t (absorbance after irradiation at different time intervals) corresponding to the test solution concentration C_o (initial concentration of stock dye solution) and C_t (remained concentration of dye solution at different time intervals). It can be seen that the absorbance of degraded MO decreases with time when the dye solution has been irradiated with the source of light for different time intervals. Therefore degradation of MO follows first-order rate kinetics as given by equation (2). The value of the rate constant ($k = 0.0143\ min^{-1}$) has been evaluated from the slope of $\ln C_o/C_t$ vs time (min) curve as given in Fig. 6 (b).

Moreover, the efficiency of ZnO NPs (B3) nanocatalyst to degrade the MO has been obtained from equation (3). Fig. 6 (c) shows the degradation efficiency (%) vs time (min) plot and the efficiency is calculated as 84.62 % at a degradation time of 180 min. Table 3 represents a comparative study on photocatalytic activity of as-synthesized ZnO NPs (B3) with respect to the reported ZnO NPs based nanocatalyst in dye degradation [54–64]. Gawade et al have reported 81 % efficiency of MO degradation under the exposure of UV light for 100 min using ZnO NPs synthesized using leaves extract of *Calotropis procera* [62]. Likewise, Karnan et al have also investigated 83.99 % efficiency of MO

Table 3
A comparative study on photocatalytic activity of as-synthesized ZnO NPs (B3) with respect to the reported ZnO NPs based nanocatalyst in dye degradation [54–64].

S. N.	Nanocatalyst	Plant Source	Dye	Light source of irradiation	Time of irradiation	Degradation efficiency %	References
1	ZnO NPs	*Garcinia mangostana*	Malachite green	Sunlight	180 min	99 %	[54]
2	ZnO NPs	*Brassia oleracea L. Var. italic*	Methylene blue	UV light	180 min	74 %	[55]
3	ZnO NPs	*Brassia oleracea L. Var. italic*	Phenol red	UV light	180 min	71 %	[55]
4	ZnO NPs	*Myristica fragrans*	Methylene blue	UV light	140 min	88 %	[56]
5	ZnO NPs	*Heliotropium indicum*	Methylene blue	Sunlight	240 min	93 %	[57]
6	ZnO NPs	*Salvadora persica*	Methylene blue	UV light	150 min	95 %	[58]
7	ZnO NPs	*Passiflora foetida*	Rhodamine B	UV light	70 min	91.06 %	[59]
8	ZnO NPs	*Bridelia retusa*	Rhodamine B	Sunlight	165 min	94.74 %	[60]
9	Ag-ZnO NPs	*Trigonella foenum-graecum*	Malachite green	Visible light	120 min	100 %	[61]
14	ZnO NPs	*Azadirachta indica*	Methyl orange	UV light	180 min	84.62 %	This work

degradation under the exposure of UV light for 120 min using ZnO NPs synthesized using peel extract of *Nephelium lappaceuml* [63]. Similar, results have been obtained with green synthesized ZnO by Varadavenkatesan et al [65]. Thus, the photocatalytic activity of MO using as-synthesized ZnO NPs (B3) is in good agreement with the reported photocatalytic activity.

$$kt = \ln\frac{C_o}{C_t} \tag{2}$$

$$Degradation\ efficiency\,(\%) = \left(\frac{C_o - C_t}{C_o}\right) \times 100... \tag{3}$$

The mechanism of MO dye degradation with ZnO NPs (B3) has been given as below (reaction steps 1–7). Herein, in the first step adsorption of dye on the surface (active sites) of ZnO NPs (B3) takes place. In the second step on exposure of UV–Visible light, the electrons (e^-) and holes (h^+) are generated. In the third step, when holes (h^+) combine with nanocatalyst ZnO NPs (B3) and consequently, the H^+ and $HO^{\cdot}$ are produced. In the fourth step, the ZnO (h^+) combine with ^-OH and generates hydroxyl radical ($HO^{\cdot}$). In the fifth step, ZnO (e^-) reacts with dissolved oxygen (O_2) in the dye solution and generates a peroxy anion radical ($O_2^{-\cdot}$). Thus hydroxyl radicals ($HO^{\cdot}$) and peroxy anion radicals (O_2^{-}) (step 6 & 7) react with dye molecules and gives intermediates products and finally carbon dioxide (CO_2) and water (H_2O) are formed in this process.

$$ZnO + dye \rightarrow ZnO\text{–}dye \tag{1}$$

$$ZnO\text{–}dye + hv\ (source\ of\ light,\ LPML) \rightarrow ZnO(e^-, h^+)\text{—}dye \tag{2}$$

$$ZnO\ (h^+) + H_2O \rightarrow ZnO(OH^{\bullet}) + H^+ \tag{3}$$

$$ZnO\ (h^+) + OH^- \rightarrow ZnO(OH^{\bullet}) \tag{4}$$

$$ZnO\ (e^-) + O_2 \rightarrow ZnO(O_2^-) \tag{5}$$

$$OH^{\bullet} + dye \rightarrow intermediate\ products \rightarrow degradation\ products \tag{6}$$

$$O_2^{-\bullet} + dye \rightarrow intermediate\ products \rightarrow degradation\ products \tag{7}$$

3.8. Electrochemical study

The electrochemical study of S3 and B3 ZnO NPs (drop cast on Pt electrode) has been performed with help of the cyclic-voltammetry technique in presence of 0.5 M Na_2SO_4 electrolyte. The cyclic-voltammogram (CV curves) are obtained at different scan rates as shown in Fig. 7 (a) and Fig. 8 (a) for S3 and B3 ZnO NPs, respectively. Moreover, Fig. 7 (b) and Fig. 8 (b) represent the specific capacitance vs scan rates curves for S3 and B3 ZnO NPs, respectively. Herein, the specific capacitance (C_s) and energy density (E) of as-synthesized S3 and B3 ZnO NPs are determined using CV curves based on the equations (4) and (5), respectively [66].

$$C_S = \frac{\int I}{mS(V_2 - V_1)} \tag{4}$$

where C_s is the specific capacitance (farad (F) per gram (g)), m is the mass of the electrode materials, I is the integrated current area and (V_2 - V_1) is the potential window and S is the voltage scan rate.

$$E = \frac{1}{2} \times \left(\frac{1000}{3600}\right) \times C_S V^2 \tag{5}$$

where, E is the energy density (watts (W) hour (h) per kilogram (kg), V is the potential window, C_s is the specific capacitance.

The C_s values are estimated as 1.5351F/g, 1.4308F/g, 1.3333F/g, 1.2485F/g and 1.1944F/g for S3 NPs (refer Table 4) and 1.2735F/g, 1.1470F/g, 1.0805F/g, 1.0422F/g and 1.0073F/g for B3 NPs (refer Table 5) at 20 mV/s, 40 mV/s, 60 mV/s, 80 mV/s and 100 mV/s, respectively. It can be seen that the C_s value decreases with increasing scan rates from 20 mV/s to 100 mV/s (refer to Fig. 7 (b) and 8 (b)) whereas, the peak current increases with the increase of scan rates (refer to Fig. 7 (a) and 8 (a)). It means as-synthesized ZnO NPs (S3/B3) have high charge storage efficiency at a lower scan rate. Our results are in good agreements with reported value for graphene oxide (2.13F/g) at 5 mV/s [67].

Furthermore, the E values are evaluated as 0.1539 Wh/kg, 0.1435 Wh/kg, 0.1337 Wh/kg, 0.1252 Wh/kg, and 0.1197 Wh/kg for S3 NPs (refer Table 4) and 0.1277 Wh/kg, 0.1150 Wh/kg, 0.1083 Wh/kg, 0.1045 Wh/kg, and 0.1010 Wh/kg for B3 NPs (refer Table 5) at 20 mV/s, 40 mV/s, 60 mV/s, 80 mV/s and 100 mV/s, respectively. The energy density values of as-synthesized ZnO NPs (S3/B3) are in good agreements with the reported values of energy density for ZnO NPs as the electrode materials [7,35]. Herein, Yadav et al have used Pt electrode drop casted with synthesized ZnO NPs whereas Rani et al have used the glassy carbon electrode (GCE) drop casted with synthesized ZnO NPs.

It is clear that the value of specific capacitance (C_s), as well as energy density (E) depends upon the synthesized material as well as the type of drop casted working electrode. Table 6 represents the comparative study of C_s and E for ZnO NPs and their nanocomposites with as-synthesized ZnO NPs (S3/B3) for supercapacitor application [68–71,7]. The specific capacitance and energy density values (C_s = 1.0–1.5F/g and E = 0.10–0.15 Wh/kg at 20–100 mV/s) of as-synthesized ZnO NPs (S3/B3) are found to be very less than the reported C_s (130–535Fg^{-1}) and E

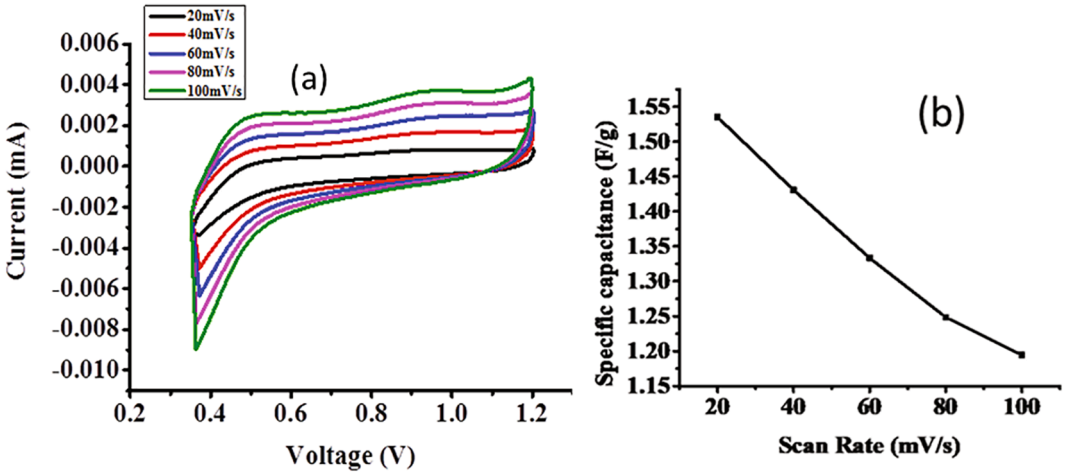

Fig. 7. (a) Cyclic Voltammetry curves of as-synthesized ZnO NPs (S3) (Potential window 0.35 V to 1.2 V), (b) Specific capacitance (C_s) vs Scan rate curve.

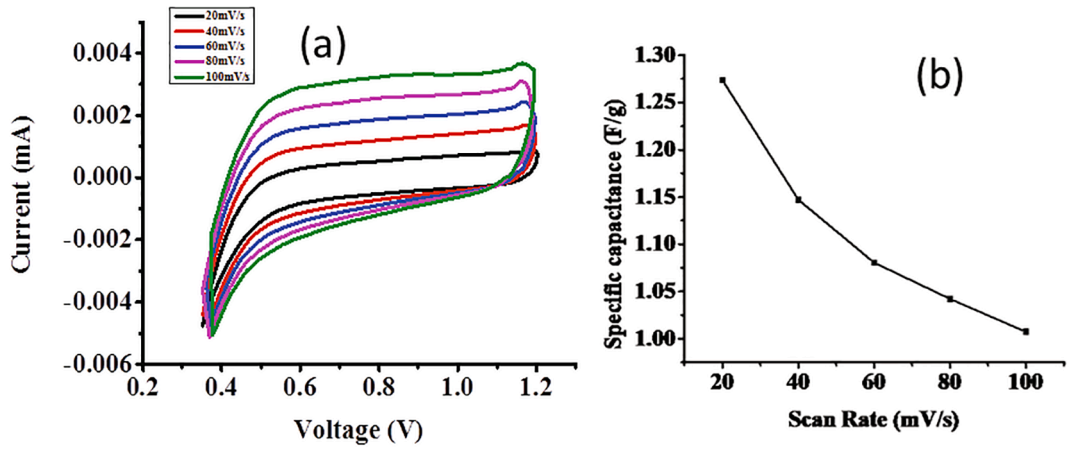

Fig. 8. (a) Cyclic Voltammetry curves of as-synthesized ZnO NPs (B3) (Potential window 0.35 V to 1.2 V), (b) Specific capacitance (C_s) vs Scan rate curve.

Table 4
Specific capacitance (C_s) and energy density (E) values of as-synthesized ZnO NPs (S3) using CV curves.

S. N.	Scan rate (mV/S)	C_s (F/g)	E (Wh/kg)
1	20	1.5351	0.1539
2	40	1.4308	0.1435
3	60	1.3333	0.1337
4	80	1.2485	0.1252
5	100	1.1944	0.1197

Table 5
Specific capacitance (C_s) and energy density (E) values of as-synthesized ZnO NPs (B3) using CV curves.

S. N.	Scan rate (mV/S)	C_s (F/g)	E (Wh/kg)
1	20	1.2735	0.1277
2	40	1.1470	0.1150
3	60	1.0805	0.1083
4	80	1.0422	0.1045
5	100	1.0073	0.1010

(8–36 Wh/kg) values. The specific capacitance value (448F/g) has been reported for the nanocomposite of graphene foam and zinc oxide (ZnO) NPs [32].

4. Conclusions

In this work, ZnO NPs (S3 nanoblocks/B3 nanobars) have been successfully synthesized using the extract of seeds/barks of *Azadirachta indica*, respectively. The maximum UV–Vis absorbance values of the as-synthesized S3/B3 NPs are obtained at about 369/367 nm and the corresponding energy bandgap are determined as 2.82/2.48 eV using tauc's plots, respectively. XRD pattern and FTIR spectra confirm hexagonal wurtzite crystalline structure and phytochemicals coating of the S3/B3 NPs, respectively. DLS (zeta potential) study displayed good colloidal stability of the as-synthesized of ZnO NPs in aqueous suspension.

The antimicrobial activity of S3 NPs is investigated with four bacteria such as *Pseudomonas aeruginosa*, *Escherichia coli*, *Staphylococcus aureus* and *Streptococcus pneumonia* respectively. MIC values indicate that as-synthesized ZnO NPs inhibit the growth of the gram-positive microbes (*Staphylococcus aureus* and *Streptococcus pneumonia*) more than the gram-negative microbes (*Pseudomonas aeruginosa, Escherichia coli*). Methyl orange dye degradation efficiency is found 84.62 % in 180 min using the as-synthesized ZnO NPs (B3). Moreover, the cyclic voltammetry study reveals that green synthesized ZnO NPs (S3/B3) are promising to be used for supercapacitor applications. Herein, specific capacitance (C_s) and energy density (E) values indicate that as-prepared S3/B3 have high charge storage efficiency at scan rate 20 mV/s as compared to scan rate at 100 mV/s. In summary, in vitro study demonstrated that green synthesized ZnO NPs (S3) can be used as an alternative source of antibiotics in future. Photocatalytic study with green synthesized ZnO NPs (B3) indicates that these NPs can be used in the degradation of pollutants in an environmentally friendly manner. The C_s/E values exhibited that S3/B3 NPs can be used as electrode material in future for supercapacitor application.

Table 6
A ccomparative electrochemical study of specific capacitance (C_s) and energy density (E) values of reported green synthesized ZnO NPs and their nanocomposites for supercapacitor application [68–72,7].

S. N.	Electrode materials	Plant Source	C_s (F/g)	E (Wh/kg)	References
1	ZnO/styrene maleic anhydride nanocomposite	*Piper nigrum*	268.5 (at 0.1 A/g)	13.42	68
2	ZnO/reduced graphene oxide nanocomposite	*Eclipta prostrata*	130 (at 1.0A/g)	–	69
3	ZnO-$CoMoO_4$ nanocomposite	*Egira cognata*	294.7 (at 2 mV/s)	8.0	70
4	Reduced graphene oxide/ZnO nanocomposite	*Lagenaria siceraria*	398 (at 10 mV/s)	–	71
5	ZnO NPs	*Euphorbia cognate*	336.12 (at 10 mV/s)	–	71
6	ZnO–Co_3O_4	*phyto-organic complex*	165		72
7	ZnO NPs	*Tabernaemontana divericata*	535.71 (at 20 mV/s)	36.45	6
8	ZnO NPs (S3/B3)	*Azadirachta indica*	1.0–1.5 (at 20–100 mV/s)		This work

Declaration of Competing Interest

The authors declare that they have no known competing financial interests or personal relationships that could have appeared to influence the work reported in this paper.

Acknowledgment

The authors wish to thank Principal, Miranda House, University of Delhi for providing lab facility to carry out this research work. The authors wish to thank University Scientific Instrumentation Centre (USIC), University of Delhi, India for providing SEM, EDS and XRD facilities. Dipak Maity would like to thank the University of Petroleum and Energy Studies (UPES) for providing all the support. Kalawati Saini and Mona Saini also deeply acknowledge to Department of Biotechnology (DBT), New Delhi, India for providing fund under INDO-US FOLDSCOPE scheme (Sanction order No. BT/IN/Indo/Foldscope/39/2015 dated: 20.03.2018). Sapna Yadav thanks to CSIR, New Delhi for getting junior research fellowship (Ref. No. 08/700/(0004)/2019-EMR-1). Kalawati Saini would like to thank Dr. Amrita Tripathi Sheikh, Associate Professor, Miranda House, University of Delhi for her constant encouragement and support.

References:

[1] A. Taşdemir, R. Aydin, A. Akkaya, N. Akman, Y. Altinay, H. Çetin, B. Şahin, A. Uzun, E. Ayyildiz, A green approach for the preparation of nanostructured zinc oxide: Characterization and promising antibacterial behaviour, Ceram. Int. 47 (14) (2021) 19362–19373, https://doi.org/10.1016/j.ceramint.2021.03.273.

[2] J. Li, Y. Li, H. Wu, S. Naraginti, Y. Wu, Facile synthesis of ZnO nanoparticles by *Actinidia deliciosa* fruit peel extract: Bactericidal, anticancer and detoxification properties, Environ. Res. 200 (2021), 111433, https://doi.org/10.1016/j.envres.2021.111433.

[3] M. Govarthanan, P. Srinivasan, T. Selvankumar, V. Janaki, F. A. Al-Misned, H. A. El-Serehy, W. Kim, S. Kamala-Kannan, Utilization of funnel-shaped ivory flowers of *Candelabra cactus* for zinc oxide nanoparticles synthesis and their in-vitro anticancer and antibacterial activity, Mater. Lett. 273 (2020) 127951. https://doi.org/10.1016/j.matlet.2020.127951.

[4] N. Rani, K. Saini, Biogenic Metal and Metal Oxides Nanoparticles as Anticancer Agent: A Review, IOP Conf. Ser.: Mater. Sci. Eng. 1225 (1) (2022), 012043.

[5] H.-K. Seo, H.-S. Shin, Study on the photocatalytic activity of ZnO nanodisks for the degradation of Rhodamine B dye, Mater lett. 159 (2015) 265–268, https://doi.org/10.1016/j.matlet.2015.06.094.

[6] A. Hamrouni, N. Moussa, F. Parrino, A. Di Paola, A. Houas, L. Palmisano, L, Palmisano, Sol-gel synthesis and photocatalytic activity of ZnO-SnO_2 nanocomposites, J Mol Catal a Chem. 390 (2014) 133–141.

[7] N. Rani, M. Saini, S. Yadav, K. Gupta, K. Saini, M. Khanuja, High performance Supercapacitor based on rod shaped ZnO Nanostructure electrode, AIP Conf. Proc. 2276 (2020), 020042, https://doi.org/10.1063/5.0026084.

[8] M. Bayrami, A. Bayrami, A. Habibi-Yangjeh, M.S. Shafeeyan, S. Feizpoor, F. M. Arvanagh, M.R. Nourani, R.A. Taheri, Biologically-synthesised ZnO/CuO/Ag nanocomposite using *propolis* extract and coated on the gauze for wound healing applications, IET Nanobiotechnol. 14 (7) (2020) 548–554, https://doi.org/10.1049/iet-nbt.2020.0024.

[9] A. Yu, J. Qian, H. Pan, Y. Cui, M. Xu, L. Tu, Q. Chai, X. Zhou, Microlotus constructed by Fe-doped ZnO hierarchically porous nanosheets: preparation, characterization and gas sensing property, Sen. Actuators B Chem. 158 (2011) 9–16.

[10] C. Jayaseelan, A. Abdul Rahumana, A. Vishnu Kirthi, S. Marimuthua, T. Santhoshkumar, A. Bagavana, K. Gaurav, L. Karthik, K.V. Bhaskara Rao, Novel microbial route to synthesize ZnO nanoparticles using *Aeromonas hydrophila* and their activity against pathogenic bacteria and fungi. Spectrochim Acta A Mol Biomol, Spectro. 90 (2012) 78–84, https://doi.org/10.1016/j.saa.2012.01.006.

[11] R. Elilarassi, G. Chandrasekaran, Synthesis and optical properties of Ni-doped zinc oxide nanoparticles for optoelectronic applications, Optoelectron. Lett. 6 (1) (2010) 6–10.

[12] M.-P. Lu, J. Song, M.-Y. Lu, M.-T. Chen, Y. Gao, L.-J. Chen, Z.L. Wang, Piezoelectric nanogenerator using p-type ZnO nanowire arrays, Nano Lett. 9 (3) (2009) 1223–1227.

[13] H. Padalia, S. Chanda, Characterization, antifungal and cytotoxic evaluation of green synthesized zinc oxide nanoparticles using *Ziziphus nummularia* leaf extract, Artif. Cells Nanomed. Biotechnol. 45(8) (2017) 1751-1761. https://doi.org/10.1080/21691401.2017.1282868.

[14] S.S. Sana, D.V. Kumbhakar, A. Pasha, S.C. Pawar, A.N. Grace, R.P. Singh, V.-H. Nguyen, Q.V. Le, W. Peng, *Crotalaria verrucosa* Leaf Extract Mediated Synthesis of Zinc Oxide Nanoparticles: Assessment of Antimicrobial and Anticancer Activity, Molecules 25 (21) (2020) 4896.

[15] M. Martínez-Carmona, C. Marina, G. Yurii, V. Regí Maria, ZnO Nanostructures for Drug Delivery and Theranostic Applications, Nanomaterials 8 (2018) 268.

[16] M. Li, L. Zhu, D. Lin, Toxicity of ZnO Nanoparticles to Escherichia coli: Mechanism and the Influence of Medium Components, Environ. Sci. Technol. 45 (5) (2011) 1977–1983, https://doi.org/10.1021/es102624t.

[17] R. Brayner, R. Ferrari-Iliou, N. Brivois, S. Djediat, M.F. Benedetti, F. Fiévet, Toxicological Impact Studies Based on *Escherichia coli* Bacteria in Ultrafine ZnO Nanoparticles, Colloidal Medium Nano Lett. 6 (4) (2006) 866–870, https://doi.org/10.1021/nl052326h.

[18] G. Sharmila, M. Thirumarimurugan, C. Muthukumaran, Green synthesis of ZnO nanoparticles using *Tecoma castanifolia* leaf extract: Characterization and evaluation of its antioxidant, bactericidal and anticancer activitie, Microchem. J. 145 (2019) 578–587.

[19] M. Ramesh, M. Anbuvannan, G. Viruthagiri, Green synthesis of ZnO nanoparticles using *Solanum nigrum* leaf extract and their antibacterial activity, Spectrochim. Acta A. Mol. Biomol, Spectrosc. 136 (2015) 864–870, https://doi.org/10.1016/j.saa.2014.09.105.

[20] Z. Zhong, Z. Xu, T. Sheng, J. Yao, W. Xing, Y. Wang, Unusual Air Filters with Ultrahigh Efficiency and Antibacterial Functionality Enabled by ZnO Nanorods, ACS Appl. Mater. Interfaces 7 (38) (2015) 21538–21544, https://doi.org/10.1021/acsami.5b06810.

[21] R. Dobrucka, J. Długaszewska, Biosynthesis and antibacterial activity of ZnO nanoparticles using *Trifolium pratense* flower extract, Saudi, J. Biol. Sci. 23 (4) (2016) 517–523.

[22] F.M. Arvanag, A. Bayrami, A.H. Yangjeh, S.R. Pouran, A comprehensive study on antidiabetic and antibacterial activities of ZnO nanoparticles biosynthesized using *Silybum marianum* L seed extract, Mater Sci Eng C. 97 (2019) 397–405, https://doi.org/10.1016/j.msec.2018.12.

[23] N. Asif, S. Fatima, M. A. Md. Aziz, Shehzadi, A. Zaki, T. Fatma, Biofabrication and characterization of cyanobacteria derived ZnO NPs for their bioactivity comparison with commercial chemically synthesized nanoparticles, Bioorg. Chem. 113 (2021) 104999. https://doi.org/10.1016/j.bioorg.2021.104999.

[24] K.K. Das, L. Paramanik, K. Parida, An insight to band-bending mechanism of polypyrrole sensitized B-rGO/$ZnFe_2O_4$ p-n heterostructure with dynamic charge transfer for photocatalytic applications, Int. J. Hydrog. Energy. 46 (48) (2021) 24484–24500.

[25] T. Lv, L.K. Pan, X.J. Liu, Z. Sun, Enhanced photocatalytic degradation of methylene blue by ZnO-reduced graphene oxide-carbon nanotube composites synthesized via microwave-assisted reaction, Catal. Sci. Technol. 2 (2012) 2297–2301.

[26] P. Gao, K. Ng, D.D. Sun, Sulfonated graphene oxide-ZnO-Ag photocatalyst for fast photodegradation and disinfection under visible light, J. Hazard. Mater. 262 (2013) 826–835.

[27] Y. Gu, G. Teng, X. Jin, L. Wang, Z. Qiang, W. Ma, C. Zhang, Shape-Controlled Synthesis of Coral-like ZnO/C-$ZnFe_2O_4$ Hierarchical Structures and Their Improved Photocatalytic Antibacterial Efficiency under Visible Light Illumination, Indust. Eng. Chem. Res. 59 (24) (2020) 11219–11231, https://doi.org/10.1021/acs.iecr.0c00939.

[28] R.C. Justin, R. Murugesan, R. Manikandan, Y.S. Ju, H. Koot, S. Yu, P. Yeup, H. S. Jun, B.C. Kim, Two-Dimensional Planar Supercapacitor Based on Zinc Oxide/Manganese Oxide Core/Shell Nano-architecture, J. Electrochimica Acta 247 (2017) 949–957.

[29] M. Saghafi, S. Zangeneh, Zn-Co oxide electrode with excellent capacitive behavior for using supercapacitor application, Curr. Appl. Phys. 19 (6) (2019) 745–755.

[30] J.H. Zheng, R.M. Zhang, P.E. Yu, X.G. Wang, Binary transition metal oxides (BTMO) (Co-Zn, Co-Cu) synthesis and high supercapacitor performance, J. Alloys compd. 772 (2019) 359–365.

[31] J. Sun, S. Li, X. Han, F. Liao, Y. Zhang, G. Li, H. Chen, C. Xu, Rapid hydrothermal synthesis of snowflake-like $ZnCo_2O_4$/ZnO mesoporous microstructures with excellent electrochemical performances, Int. Ceramics 45 (9) (2019) 12243–12250.

[32] S. Kasap, I. Ismet, S. Kaya, E.E. Repp, Superbat: battery-like supercapacitor utilized by graphene foam and zinc oxide (ZnO) electrodes induced by structural defects, Nanoscale Adv. 1 (2019) 2586–2597.

[33] M.Y. Ho, P.S. Khiew, D. Isa, T.K. Tan, W.S. Chiu, C.H. Chia, A review of metal oxide composite electrode materials for electrochemical capacitors, NANO 09 (2014) 1430002–1430026.

[34] T. Kou, B. Yao, T. Liu, Y. Li, Recent advances in chemical methods for activating carbon and metal oxide based electrodes for supercapacitors, J. Mater. Chem. A 5 (33) (2017) 17151–17173.

[35] S. Yadav, N. Rani, K. Saini, Green synthesis of ZnO and CuO NPs using *Ficus benghalensis* leaf extract and their comparative study for electrode materials for high performance supercapacitor application, Mater. Today:. Proc. 49 (2022) 2124–2130.

[36] M.S. Yadav, N. Singh, S.M. Bobade, Zinc oxide nanoparticles and activated charcoal-based nanocomposite electrode for supercapacitor application, Ionics 24 (11) (2018) 3611–3630.

[37] L Garcia, Broth Microdilution MIC Test, In Clinical Microbiology Procedures Handbook, 3rd Edition. ASM Press, Washington, DC. (2010) 25-41. doi: 10.1128/9781555817435.ch5.2.

[38] A. Muniyan, K. Ravi, U. Mohan, R. Panchamoorthy, Characterization and in vitro antibacterial activity of saponin-conjugated silver nanoparticles against bacteria that cause burn wound infection World, J. Microbiol. Biotechnol. 33 (7) (2017) 1–12.

[39] G. Khara, H. Padalia, P. Moteriya, S. Chanda, Peltophorum pterocarpum Flower-Mediated Synthesis, Characterization, Antimicrobial and Cytotoxic Activities of ZnO Nanoparticles, Arab. J. Sci. Eng. 43 (2018) 3393–3401, https://doi.org/10.1007/s13369-017-2875-6.

[40] H. Padalia, S. Chanda, Characterization, antifungal and cytotoxic evaluation of green synthesized zinc oxide nanoparticles using *Ziziphus nummularia* leaf extract, Artif Cells Nanomed. Biotechnol. 45(8) (2017) 1751-1761. https://doi.org/10.1080/21691401.2017.1282868.

[41] C. Jayaseelan, A. Abdul Rahumana, A. Vishnu Kirthi, S. Marimuthua, T. Santhoshkumar, A. Bagavana, K. Gaurav, L. Karthik, K.V. Bhaskara Rao, Novel microbial route to synthesize ZnO nanoparticles using *Aeromonas hydrophila* and their activity against pathogenic bacteria and fungi, Spectrochim Acta A Mol Biomol, Spectro. 90 (2012) 78–84, https://doi.org/10.1016/j.saa.2012.01.006.

[42] M.A.M. Khan, S. Kumar, A.N. Alhazaa, M.A. Al-Gawati, Modifications in structural, morphological, optical and photocatalytic properties of ZnO: Mn nanoparticles by sol-gel protocol, Mater. Sci. Semiconductor Proc. 87 (2018) 134–141, https://doi.org/10.1016/j.mssp.2018.07.016.
[43] C.A. Soto-Robles, P.A. Luque, C.M. Gomez-Gutierrez, O. Nava, A.R. Vilchis-Nestor, E. Lugo-Medina, R. Ranjithkumar, A. Castro-Beltran, Study on the effect of the concentration of Hibiscus sabdariffa extract on the green synthesis of ZnO nanoparticles, Results Phys. 15 (2019), 102807, https://doi.org/10.1016/j.rinp.2019.102807.
[44] R. Salehi, M. Arami, N.M. Mahmoodi, H. Bahrami, S. Khorramfar, Novel biocompatible composite (Chitosan-ZnO nanoparticles): preparation, characterization and dye adsorption properties, Colloid Surf. B 80 (2010) 86–93, https://doi.org/10.1016/j.colsurfb.2010.05.039.
[45] M.J. Akhtar, M. Ahamed, S. Kumar, M.M. Khan, J. Ahmad, S.A. Alkokayan, Zinc Oxide nanoparticles selectively induce apoptosis in human cancer cells through reactive oxygen species, Int. J. Nanomed. 7 (2012) 845–857, https://doi.org/10.2147/IJN.S29129.
[46] R.M. Asik, B. Gowdhami, M.S. Mohamed Jaabir, G. Archunan, N. Suganthy, Anticancer potential of zinc oxide nanoparticles against cervical carcinoma cells synthesized via biogenic route using aqueous extract of *Gracilaria edulis*, Mater. Sci. Eng. C 103 (2019), 109840.
[47] M.I. Khan, N. Fatima, M. Shakil, M.B. Tahir, K.N. Riaz, M. Rafique, T. Iqbal, K. Mahmood, Investigation of in-vitro antibacterial and seed germination properties of green synthesized pure and nickel doped ZnO nanoparticles, Phys. B Phys. Condens. Matter 601 (2021), 412563.
[48] H. Chandra, D. Patel, P. Kumari, J.S. Jangwan, S. Yadav, Phyto-mediated synthesis of zinc oxide nanoparticles of *Berberis aristata*: Characterization, antioxidant activity and antibacterial activity with special reference to urinary tract pathogens, Mater. Sci. Eng. C 102 (2019) 212–220.
[49] V. Ganesan, M. Hariram, S. Vivekanandhan, S. Muthuramkumar, *Periconium sp.* (endophytic fungi) extract mediated sol-gel synthesis of ZnO nanoparticles for antimicrobial and antioxidant applications, Mater. Sci. Semicond. Process. 105 (2020), 104739.
[50] A. Król, V. Railean-Plugaru, P. Pomastowski, B. Buszewski, Phytochemical investigation of *Medicago sativa* L. extract and its potential as a safe source for the synthesis of ZnO nanoparticles: The proposed mechanism of formation and antimicrobial activity, Phytochem. Lett. 31 (2019) 170–180.
[51] M. Khatami, R.S. Varma, N. Zafarnia, H. Yaghoobi, M. Sarani, V.G. Kumar, Applications of green synthesized Ag, ZnO and Ag/ZnO nanoparticles for making clinical antimicrobial wound-healing bandages, Sustain. Chem. Pharm. 10 (2018) 9–15.
[52] M.M. Khan, M.H. Harunsani, A.L. Tan, M. Hojamberdiev, Y.A. Poi, N. Ahmad, Antibacterial Studies of ZnO and Cu-Doped ZnO Nanoparticles Synthesized Using Aqueous Leaf Extract of *Stachytarpheta jamaicensis*, BionanoScience 10 (4) (2020) 1037–1048.
[53] M. Barani, M. Masoudi, M. Mashreghi, A. Makhdoumi, H. Eshghi, Cell-free extract assisted synthesis of ZnO nanoparticles using aquatic bacterial strains: Biological activities and toxicological evaluation, Int. J. Pharm. 606 (2021), 120878, https://doi.org/10.1016/j.ijpharm.2021.120878.
[54] M. Aminuzzaman, L.P. Ying, W.S. Goh, A. Watanabe, Green synthesis of zinc oxide nanoparticles using aqueous extract of *Garcinia mangostana* fruit pericarp and their photocatalytic activity, Bull. Mater. Sci. 41 (2018) 50.
[55] J. Osuntokun, D.C. Onwudiwe, E.E. Ebenso, Green synthesis of ZnO nanoparticles using aqueous *Brassica oleracea L. var. italica* and the photocatalytic activity, Green Chem. Lett. Rev. 12 (4) (2019) 444–457.
[56] S. Faisal, H. Jan, S.A. Shah, S. Shah, A. Khan, M.T. Akbar, M. Rizwan, F. Jan, N. Wajidullah, A. Akhtar, S.S. Khattak, Green Synthesis of Zinc Oxide (ZnO) Nanoparticles Using Aqueous Fruit Extracts of *Myristica fragrans*: Their Characterizations and Biological and Environmental Applications, ACS Omega 6 (2021) 9709–9722.
[57] U. Wijesinghe, G. Thiripuranathar, F. Menaa, H. Iqbal, A. Razzaq, H. Almukhlifi, Green Synthesis Structural Characterization and Photocatalytic Applications of ZnO Nanoconjugates Using Heliotropium indicum, Catalysts 11 (2021) 831.
[58] F.A. Alharthi, A.A. Alghamdi, A.A. Alothman, Z.M. Almarhoon, M.F. Alsulaiman, N. Al-Zaqri, Green Synthesis of ZnO Nanostructures Using *Salvadora Persica* Leaf Extract: Applications for Photocatalytic Degradation of Methylene Blue Dye, Crystals 10 (2020) 441.
[59] M. Khan, P. Ware, N. Shimpi, Synthesis of ZnO nanoparticles using peels of *Passifora foetida* and study of its activity as an efficient catalyst for the degradation of hazardous organic dye, SN Appl. Sci. 3 (2021) 528.
[60] R. Vinayagam, S. Pai, T. Varadavenkatesan, A. Pugazhendhi, R. Selvaraj, Characterization and photocatalytic activity of ZnO nanoflowers synthesized using *Bridelia retusa* leaf extract, Appl. Nanosci. (2021), https://doi.org/10.1007/s13204-021-01816-5.
[61] Z. Noohpisheha, H. Amiri, S. Farhadi, A. Mohammadi-gholami, Green synthesis of Ag-ZnO nanocomposites using *Trigonella foenum-graecum* leaf extract and their antibacterial, antifungal, antioxidant and photocatalytic properties, Spectrochim. Acta A Mol. Biomol. Spectrosc. 240 (2020), 118595, https://doi.org/10.1016/j.saa.2020.118595.
[62] V.V. Gawade, N.L. Gavade, H.M. Shinde, S.B. Babar, A.N. Kadam, K.M. Garadkar, Green synthesis of ZnO nanoparticles by using *Calotropis procera* leaves for the photodegradation of methyl orange, J Mater Sci: Mater Electron 28 (18) (2017) 14033–14039.
[63] T. Karnan, S.A.S. Selvakumar, Biosynthesis of ZnO nanoparticles using rambutan *(Nephelium lappaceu*m L.) peel extract and their photocatalytic activity on methyl orange dye, J. Mol. Struct. 1125 (2016) 358–365.
[64] C.A. Soto-Robles, O. Nava, L. Cornejoa, E. Lugo-Medina, A.R. Vilchis-Nestor, A. Castro-Beltránd, P.A. Luque, Biosynthesis, characterization and photocatalytic activity of ZnO nanoparticles using extracts of *Justicia spicigera* for the degradation of methylene blue, J. Mol. Struct. 1225 (2021), 129101.
[65] T. Varadavenkatesan, E. Lyubchik, S. Pai, A. Pugazhendhi, R. Vinayagam, R. Selvaraj, Photocatalytic degradation of Rhodamine B by zinc oxide nanoparticles synthesized using the leaf extract of *Cyanometra ramiflora*, J. Photochem. Photobiol. B: Biol. 199 (2019) 111621.
[66] L.F. Aval, M. Ghoranneviss, G.B. Pour, High-performance supercapacitors based on the carbon nanotubes, graphene and graphite nanoparticles electrodes, Heliyon 4 (11) (2018) e00862.
[67] M. Saranya, R. Ramachandran, F. Wang, Graphene-zinc oxide (G-ZnO) nanocomposite for electrochemical supercapacitor applications, J. Sci.: Adv. Mater. Devices 1 (4) (2016) 454–460.
[68] J. Kalaiarasi, C. Pragathiswaran, P. Subramani, Green chemistry approach for the functionalization of reduced graphene and ZnO as efficient supercapacitor application, J. Mol. Struct. 1242 (2021), 130704.
[69] S. Chakraborty, A. Raj M, N. L. Mary, Biocompatible supercapacitor electrodes using green synthesised ZnO/Polymer nanocomposites for efficient energy storage applications, J. Energy Storage 28 (2020) 101275.
[70] I. Shaheen, K.S. Ahmad, M.A. Malik, M.D. Khan, Z. Hussian, K. Alamgir, Phyto-mediated semiconducting n-type electrode nanomaterial: structural, compositional, and supercapacitor investigations, Ionics 27 (2021) 833–843.
[71] M.I. Pratheepa, M. Lawrence, Conversion of *Lagenaria Siceraria* peel to reduced graphene oxide doped with zinc oxide nanoparticles for supercapacitor applications, Semicond. Phys. Quantum Electron. Optoelectron. 24 (02) (2021) 115–123.
[72] I. Shaheen, K.S. Ahmad, C. Zequine, R.K. Gupta, A.G. Thomas, M.A. Malik, Green synthesis of ZnO–Co_3O_4 nanocomposite using facile foliar fuel and investigation of its electrochemical behaviour for supercapacitors, New J. Chem. 44 (2020) 18281–18292, https://doi.org/10.1039/D0NJ03430D.
[73] Z. Breijyeh, B. Jubeh, R. Karaman, Resistance of Gram-Negative Bacteria to Current Antibacterial Agents and Approaches to Resolve It, Molecules*(Basel, Switzerland)* 25 (6) (2020 1340.), https://doi.org/10.3390/molecules25061340.
[74] N.K. Al-nemrawi, R.Q. Alkhatib, H. Ayyad, A. Nid''A, Formulation and characterization of tobramycin-chitosan nanoparticles coated with zinc oxide nanoparticles, Saudi Pharm J. 30 (4) (2022) 454–461, https://doi.org/10.1016/j.jsps.2022.01.016.